Supplementary Information for

Superlithiation of Non-conductive Polyimide toward High Performance Lithium Ion Batteries

Haoqi Yang,[a] Shuwu Liu,[a] Lihua Cao,[a] Shaohua Jiang,[b*] and Haoqing Hou[a*]

This PDF file includes:

Fig. S1- S11

Table S1- S2

References

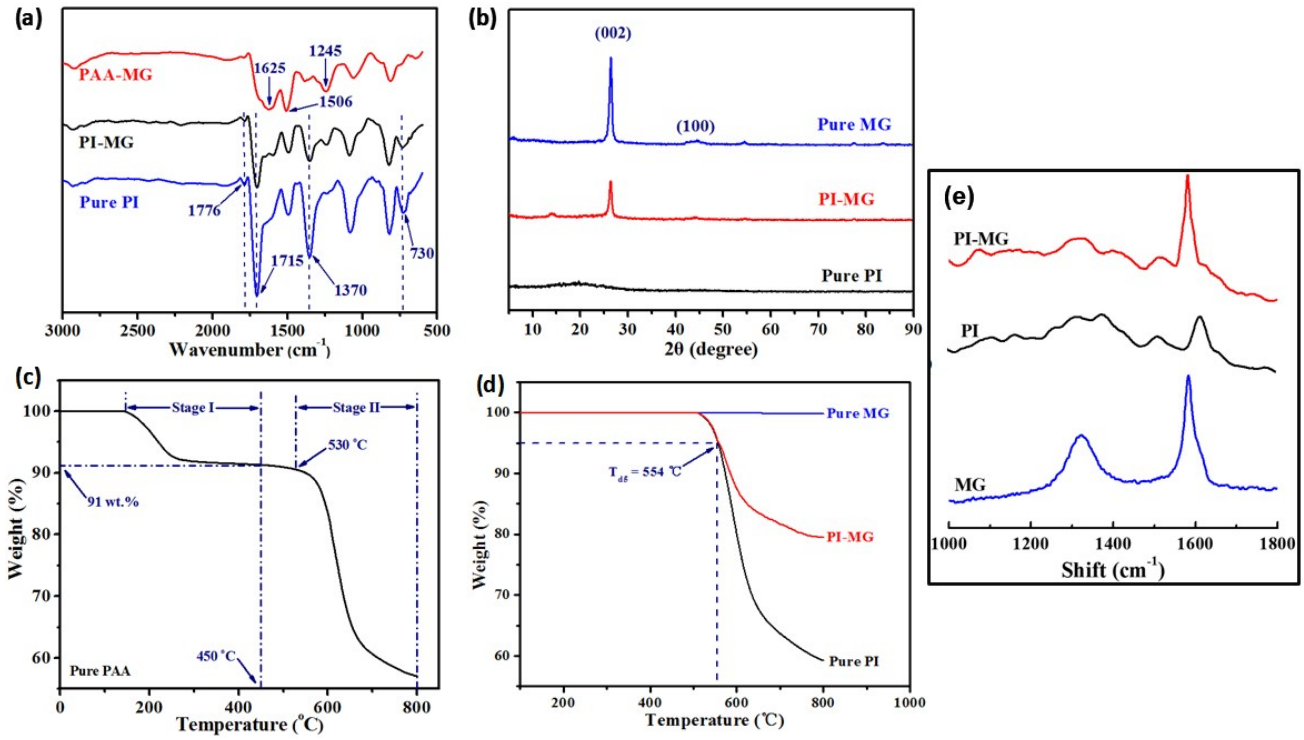

Fig. S1 (a) FT-IR spectra of PAA-MG, PI-MG and pure PI; (b) XRD patterns of pure MG , PI-MG and pure PI; (c) TGA curves of pure PAA at a heating rate of 10 °C/min in N_2;(d) TGA curves of PI-MG, pure MG and pure PI at a heating rate of 10 °C/min in N_2; (e) Raman spectra of PI-MG, pure MG and pure PI.

The imidization process from PAA-MG to PI-MG was confirmed by FT-IR spectra (Fig. S1a), and the detailed peaks of them were presented in Table S1. When the imidization temperature was around 450 °C, the peak at 1625 cm^{-1} (C=O stretching) was disappeared, and the peaks at 1776 cm^{-1} and 1715 cm^{-1} was appeared, demonstrating that the polyimide matrix was formed completely through the thermal imidization process.[1, 2] The FT-IR spectra of pure PI was also showed in Fig. S1a, it is indicated obvious absorption peaks at 1776 cm^{-1} (C=O symmetry stretching vibration in the imide), 1715 cm^{-1} (C=O asymmetry stretching vibration in the imide), 1370 cm^{-1} (C-N stretching vibration in the imide cycle) and 730 cm^{-1} (C=O bending vibration in the imide cycle), respectively.[1, 2] There is no obvious change in the absorption peaks between PI and PI-MG composite, which indicate that the multilayer graphene are successfully incorporated into polyimide particles.[3] The crystal structures of the PI-MG composite and its precursor were characterized by the XRD technique (Fig. S1b). The sharp and strong diffraction peak located at about 26.5° are observed in the XRD patterns of pure MG and PI-MG composite, which should be attributed to the feature peak (002) of graphite, and the XRD

patterns of PI-MG composite showed the same peak at 26.5° after graphene was incorporated into PI matrix, revealing that the thermal imidization process does not affect the crystal structure of the MG.

As we all know, the content of single component in the composite material is very important, especially PI, which mass content will decrease during thermal imidization process. Therefore, It's necessary to accurately calculate the mass content of PI after thermal imidization. As demonstrated in Fig. S1c, The stage I and II represent the imidization process of PAA to PI and the thermal decomposition of PI, respectively. When the degradation temperatures around 450 °C, the mass fraction of PI remained 91 wt.%, which is corresponding to the evaporation of residual solvent and the imidization process (stage I). The second step (stage II) started around 530 °C, which could be due to the decomposition of PI. In this work, 400 °C was chosen as the final imidization temperature and the annealing time was 30 min, by which the PAA would convert to PI completely. Besides, the TGA curves of PI-MG composite, pure MG and PI are observed and showed in Fig. S1d. The PI-MG sample displayed a weight loss region at 500 °C, and the degradation temperatures of 5 wt.% (T_{d5}) loss weight are around 554 °C, while the degradation temperatures (T_{d10}) of 10 wt.% loss weight are at 600.1 °C. As comparison, Pure MG has almost no degradation when temperature arrived 800 °C. Additionally, The char retention of the PI-MG composite was increased from 59.25 % to 79.56 % when compared with pure PI. Moreover, the addition of multilayer graphene improves the heat resistance of the composite and reduces the risk of the battery during operation.

Raman spectra is an effective technique to characterize the structures of materials, especially for carbon-based materials. As shown in **Fig. S1e**, Raman spectra of pure PI showed the same characteristic peaks and the strongest peak at 1612 cm^{-1} could be from the stretching of benzene rings in PI molecules. These results are the same as our previous report.[4] The spectra of MG exhibited two peaks at around 1587 and 1328 cm^{-1}, which could be assigned to the so-called G-band and D-band. This result is agreed with the characteristic peaks of graphene.[5] The Raman spectra of PI-MG showed all the peaks from pure PI and MG, indicating both components of PI and MG could be observed from PI-MG composites.

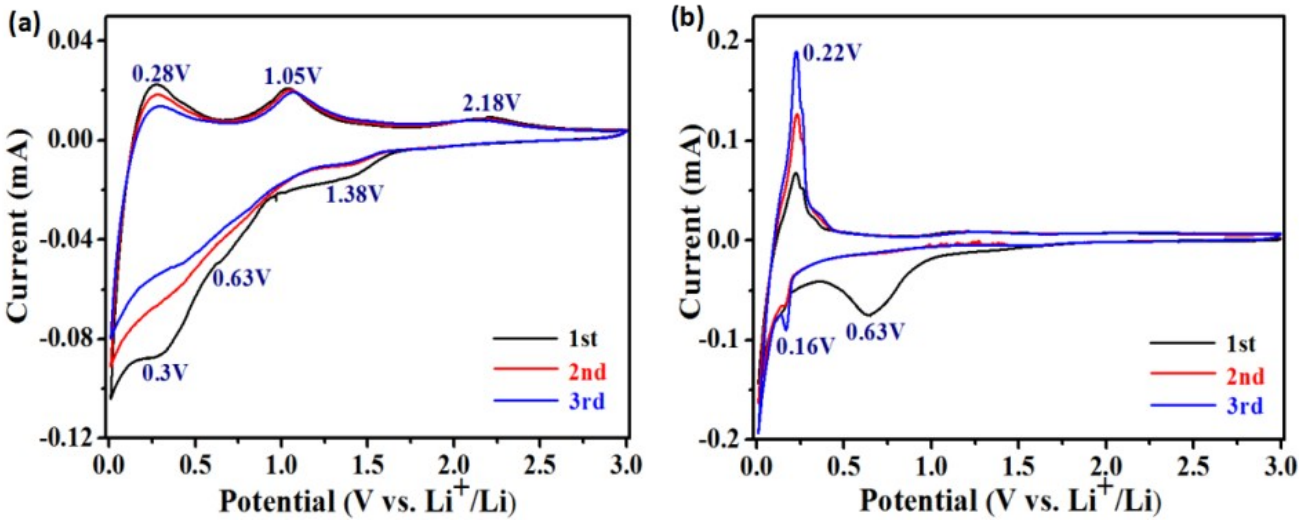

Fig. S2 Cyclic voltammetry of (a) pure PI, and (b) pure MG particle.

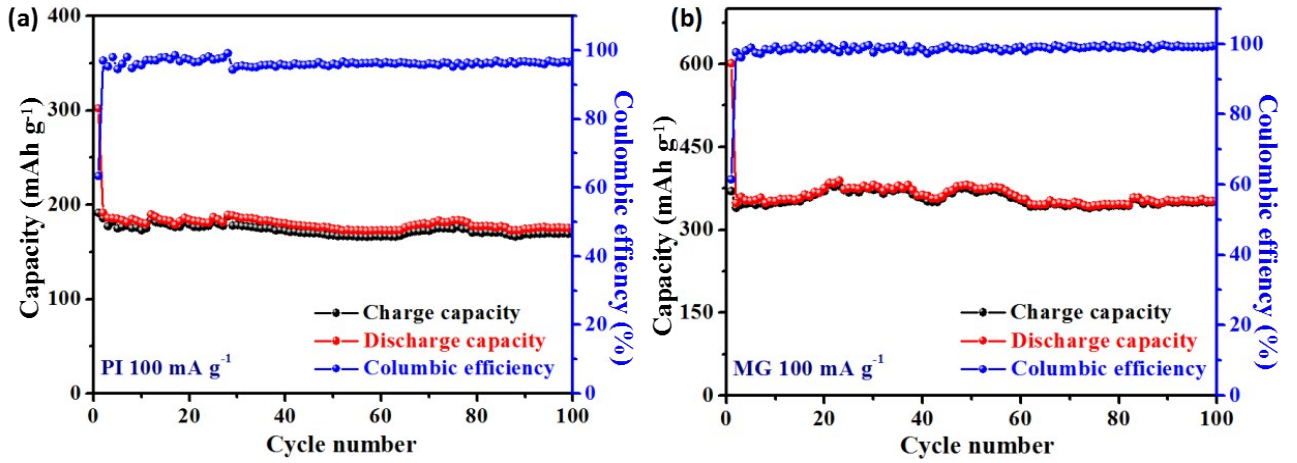

Fig. S3 Cycling performances of (a) pure PI, and (b) pure MG particle.

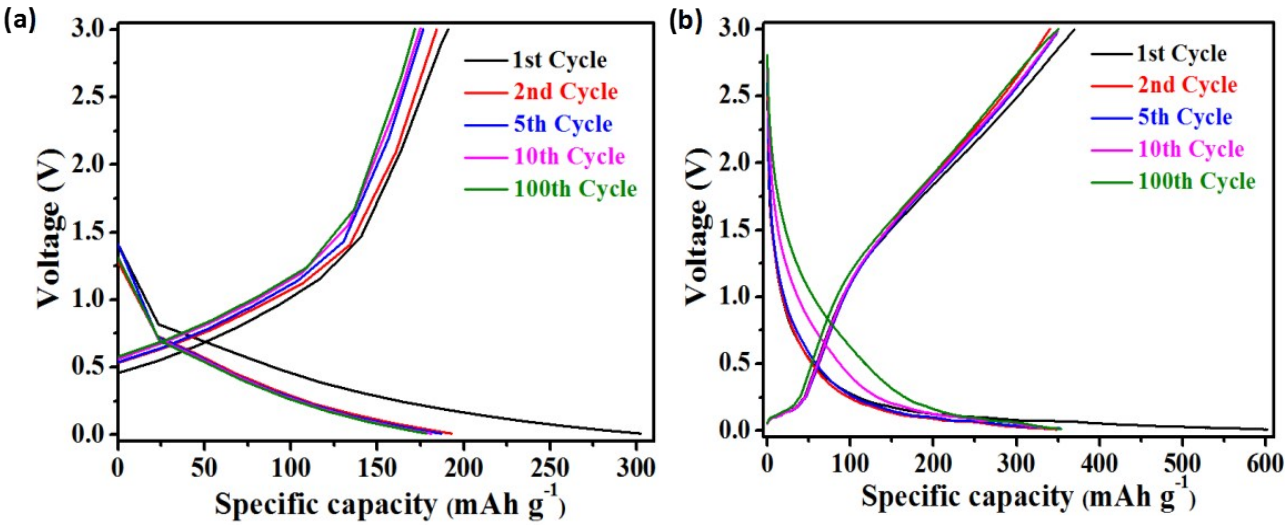

Fig. S4 Charge-discharge curves of of pure PI (a) and pure MG (b) electrode at a current density of 100 mA g^{-1}.

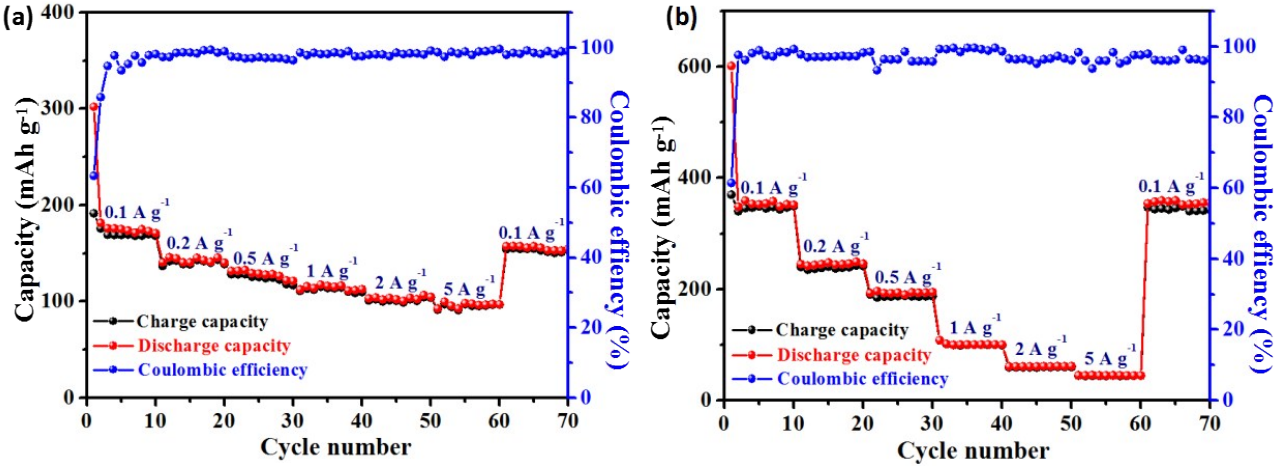

Fig. S5 Rate capability of electrode made of the pure PI (a) and pure MG (b) at current densities from 100 to 5000 mA g^{-1}.

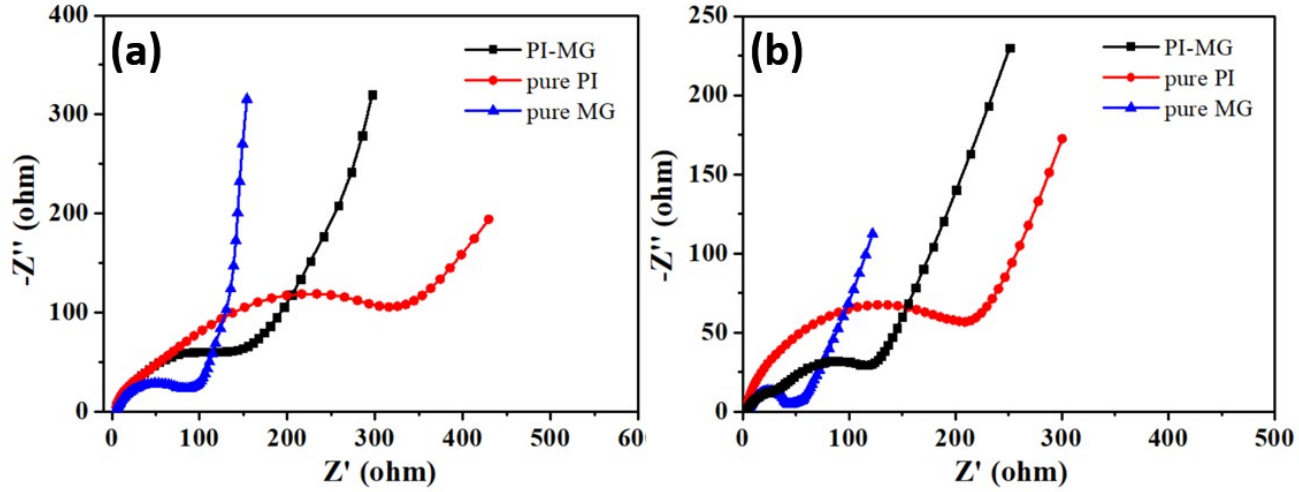

Fig. S6 Electrochemical impedance spectral (EIS) of PI-MG, pure PI, and pure MG before (a) and after (b) cycling test.

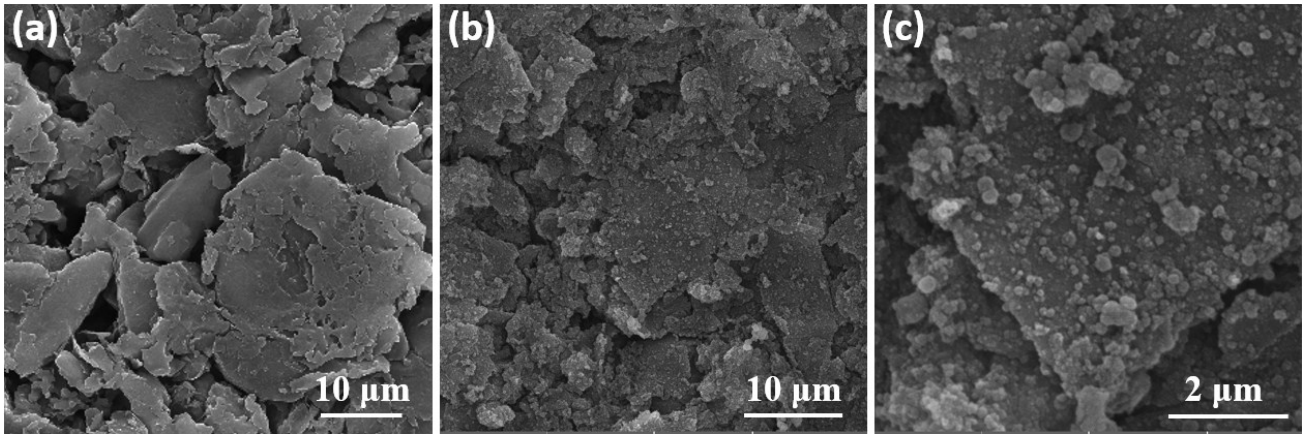

Fig. S7 SEM images of PI-MG electrodes before (a) and after (b, c) cycling test. (c) is a higher magnification image from (b).

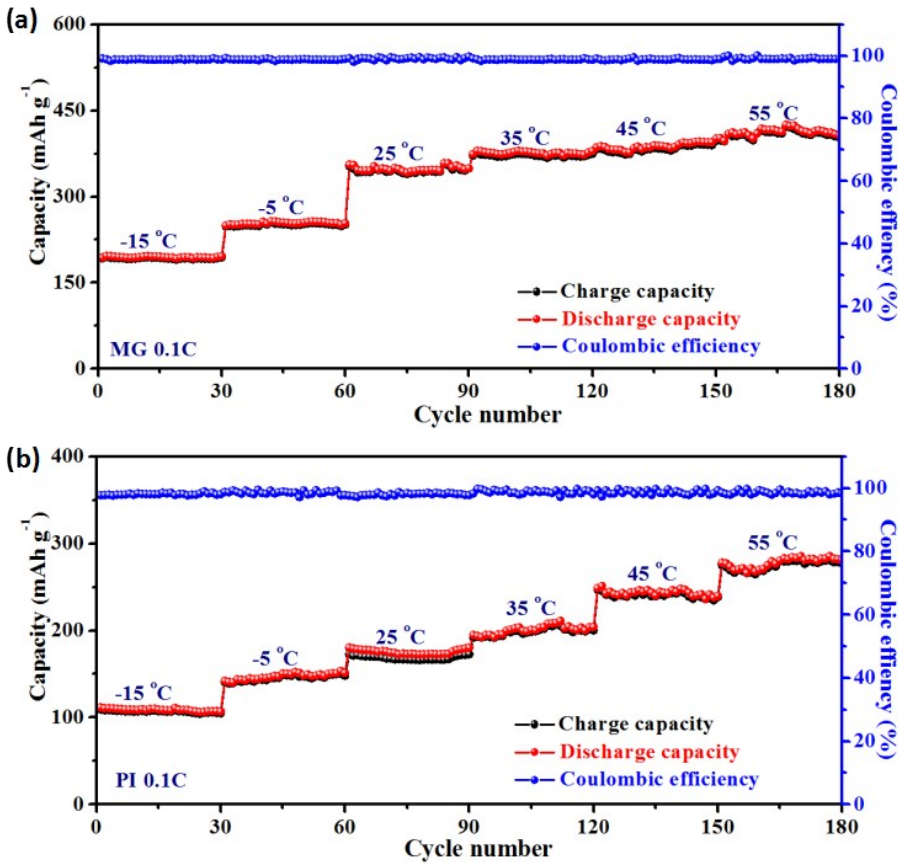

Fig. S8 Specific capacity and Coulombic efficiency of the (a) pure MG and (b) pure PI sample at various temperatures from -15 °C to 55 °C.

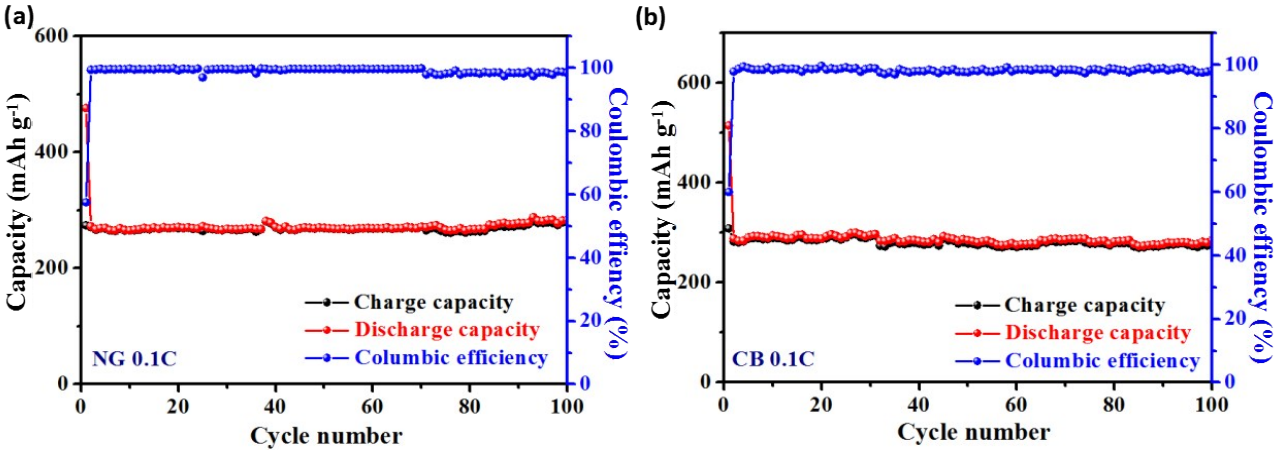

Fig. S9 Cycling performances of (a) pure NG and (b) pure CB at 0.1C.

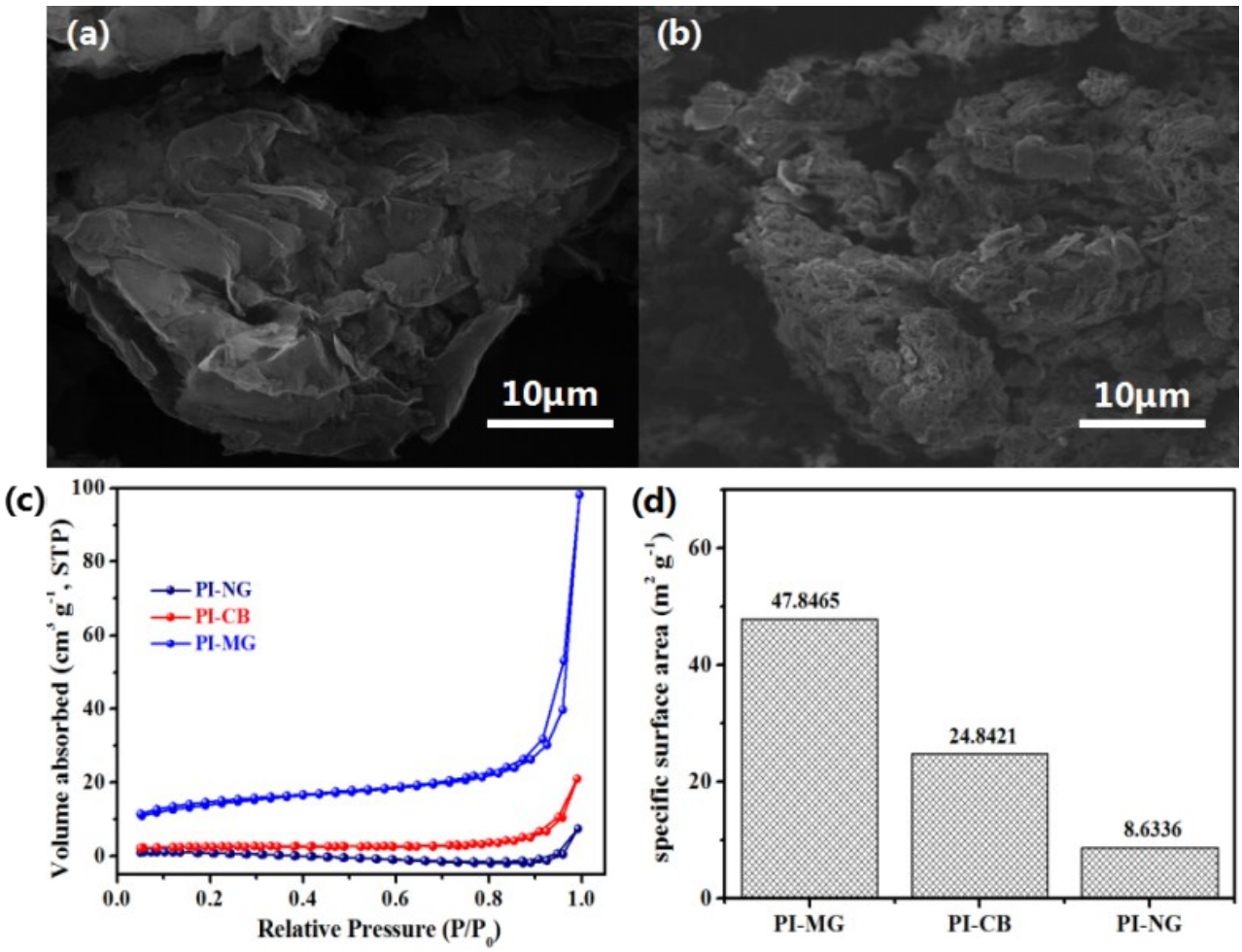

Fig. S10 SEM images of (a) PI-NG composite, and (b) PI-CB composite; Nitrogen adsorption isotherm of PI-MG, PI-CB and PI-MG composite (c), and comparison of specific surface area of these samples.

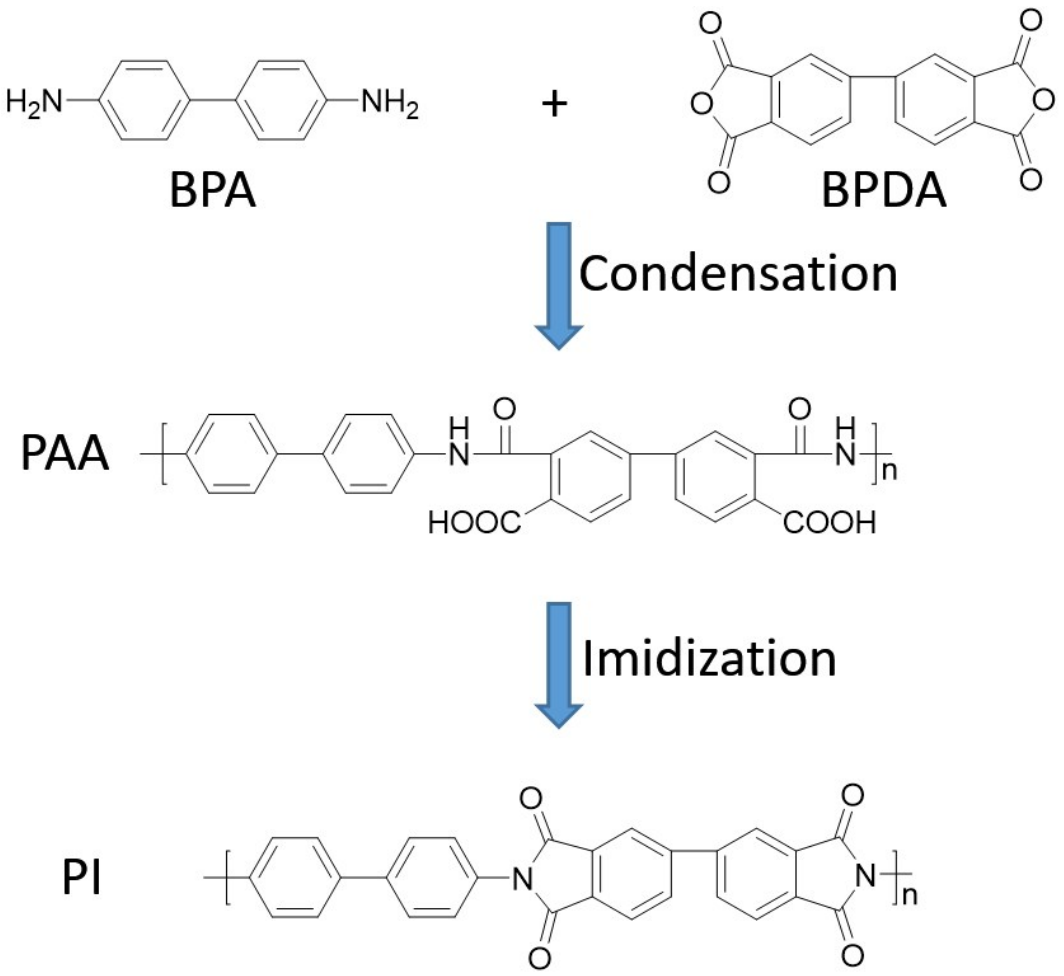

Fig. S11 Schematic diagram of the preparation of PI.

Table S1. The detailed FT-IR peaks of the PAA-MG and PI-MG.

PAA-MG		PI-MG	
Frequency (cm^{-1})	assignment	Frequency (cm^{-1})	assignment
1683	ν(C=O) amide Ⅰ	1776	ν(C=O) sym.stretching, imide Ⅰ
1625	ν(C=O) amide Ⅰ	1715	ν(C=O) asy. stretching, imide Ⅰ
1506	ν(C_6H_4)	1646	ν(C_6H_3)
1385	ν(COO^-)	1496	ν(C_6H_4)
1305	ν(C-N)	1421	ν(C6H4)
1245	ν(NH) amide Ⅲ	1370	ν(C-N-C) imide Ⅱ
1065	ν(C_6H_4)	1237	ν($(OC)_2NC$) imide Ⅲ
809	δ(COO^-)	821	ν(C_6H_3)
643	π(C=O) acid	730	ν(C-N-C) imide Ⅳ

Table S2. Performance of reported carbonyl-based organic anode materials for lithium ion batteries.

Anode structure	Mass ratio of active material in electrode	Specific capacity	Cyclic stability	Refer.
PI/MG	90%	625.7 mAh g^{-1} at 100 mA g^{-1}, 632.8 mAh g^{-1} at 0.1C.(1C=856 mA g^{-1})	612.3 mAh g^{-1} after 100 cycles	This work
PI	60%	200 mAh g^{-1} at 0.1C. (1C=405.8 mA g^{-1})	170 mAh g^{-1} after 100 cycles	[6]
PI/ Graphene nanocomposites	60%	205 mAh g^{-1} at 0.1C. (1C=367 mA g^{-1})	197 mAh g^{-1} after 10 cycles	[7]
PI/CNT nanocomposite	85%	125 mAh g^{-1} at 0.1C. (1C=273 mA g^{-1})	90 mAh g^{-1} after 300 cycles	[8]
3D graphene network-supported PI	80%	175 mAh g^{-1} at 0.1C. (1C=443 mA g^{-1})	101 mAh g^{-1} after 150 cycles at 0.5C	[9]
PI/SWNT films	100%	226 mAh g^{-1} at 0.1C. (1C=443 mA g^{-1})	175 mAh g^{-1} after 200 cycles at 0.5C	[10]
poly(anthraquinonyl sulfide) (PAQS)	40%	218 mAh g^{-1} at 0.1C. (1C=492 mA g^{-1})	198 mAh g^{-1} after 200 cycles at 0.1C	[11]
3,4,9,10-perylenetetracarboxylicacid-dianhydride (PTCDA)	80%	131 mAh g^{-1} at 100 mA g^{-1}	123 mAh g^{-1} after 200 cycles at 100 mA g^{-1}	[12]
2,5-dimethoxy-1,4-benzoquinone (DMBQ)	40%	312 mAh g^{-1} at 10 mA g^{-1}	250 mAh g^{-1} after 10 cycles at 10 mA g^{-1}	[13]

1,4,5,8-naphthalenetetracarboxylic dianhydride (NTCDA)	60%	899 mAh g^{-1} at 100 mA g^{-1}	724 mAh g^{-1} after 30 cycles at 100 mA g^{-1}	[14]
poly(5-amino-1,4-dyhydroxy anthraquinone) (PADAQ)	50%	101 mAh g^{-1} at 40 mA g^{-1}	129 mAh g^{-1} after 50 cycles at 40 mA g^{-1}	[15]

References

[1] Hatsuo Ishida, Stephen T. Wellinghoff, Eric Baer, Jack L. Koenig, Spectroscopic studies of poly[n,n'-bis(phenoxyphenyl)pyromellitimide]. 1. Structures of the polyimide and three model compounds, Macromolecules 13(4) (1980) 826-834.

[2] P. T. McKittrick, J. E. Katon, Infrared and raman group frequencies of cyclic imides, Appl. Spectrosc. 44(5) (1990) 812-817.

[3] Nguyen Dang Luong, Ulla Hippi, Juuso T. Korhonen, Antti J. Soininen, Janne Ruokolainen, Leena Sisko Johansson, Jae Do Nam, Hoang Sinh Le, Jukka Seppälä, Enhanced mechanical and electrical properties of polyimide film by graphene sheets via in situ polymerization, Polymer 52(23) (2011) 5237-5242.

[4] Shaohua Jiang, Donghua Han, Chaobo Huang, Gaigai Duan, Haoqing Hou, Temperature-induced molecular orientation and mechanical properties of single electrospun polyimide nanofiber, Mater. Lett. 216 (2018) 81-83.

[5] L. M. Malard, M. A. Pimenta, G. Dresselhaus, M. S. Dresselhaus, Raman spectroscopy in graphene, Phys. Rep. 473(5) (2009) 51-87.

[6] Zhiping Song, Hui Zhan, Yunhong Zhou, Polyimides: Promising energy-storage materials, Angewandte Chemie 122(45) (2010) 8622-8626.

[7] Zhiping Song, Terrence Xu, Mikhail L. Gordin, Ying-Bing Jiang, In-Tae Bae, Qiangfeng Xiao, Hui Zhan, Jun Liu, Donghai Wang, Polymer–graphene nanocomposites as ultrafast-charge and -discharge cathodes for rechargeable lithium batteries, Nano Letters 12(5) (2012) 2205-2211.

[8] Haiping Wu, Kai Wang, Yuena Meng, Kun Lu, Zhixiang Wei, An organic cathode material based on a polyimide/cnt nanocomposite for lithium ion batteries, J. Mater. Chem. A 1(21) (2013) 6366-6372.

[9] Y Meng, H Wu, Y Zhang, Z Wei, A flexible electrode based on a three-dimensional graphene network-supported polyimide for lithium-ion batteries, Journal of Materials Chemistry A 2(28) (2014) 10842-10846.

[10] H. Wu, S. A. Shevlin, Q. Meng, W. Guo, Y. Meng, K. Lu, Z. Wei, Z. Guo, Flexible and binder-free organic cathode for high-performance lithium-ion batteries, Advanced Materials 26(20) (2014) 3338-3343.

[11] Zhiping Song, Hui Zhan, Yunhong Zhou, Anthraquinone based polymer as high performance cathode material for rechargeable lithium batteries, Chemical Communications (4) (2009) 448-450.

[12] Han X., Chang C., Yuan L., Sun T., Sun J., Aromatic carbonyl derivative polymers as high‐performance li‐ion storage materials, Adv. Mater. 19(12) (2007) 1616-1621.

[13] Masaru Yao, Hiroshi Senoh, Shin Ichi Yamazaki, Zyun Siroma, Tetsuo Sakai, Kazuaki Yasuda, High-capacity organic positive-electrode material based on a benzoquinone derivative for use in rechargeable lithium batteries, Journal of Power Sources 195(24) (2010) 8336-8340.
[14] X. Han, G Qing, J. Sun, T. Sun, How many lithium ions can be inserted onto fused c6 aromatic ring systems?, Angewandte Chemie 51(21) (2012) 5147.
[15] Lei Zhao, Weikun Wang, Anbang Wang, Keguo Yuan, Shi Chen, Yusheng Yang, A novel polyquinone cathode material for rechargeable lithium batteries, Journal of Power Sources 233(233) (2013) 23-27.